Key Engineering Materials
ISSN: 1662-9795, Vol. 988, pp 3-10
doi:10.4028/p-QY3Qy5
© 2024 The Author(s). Published by Trans Tech Publications Ltd, Switzerland.
Submitted: 2023-11-20
Revised: 2024-03-07
Accepted: 2024-03-20
Online: 2024-09-27

Prediction of Damage Behavior of Casting Aluminum Components Considering Inhomogeneous Properties

Yuling Lang[1,a*], Dongzhi Sun[2,b], Zhihua Zhu[1,c], Xiang Ci[1,d], Decai Kong[1,e], Haibo Qiao[1,f], Wenbo Wang[1,g]

[1]CITIC Dicastal Co., Ltd, No 185, Longhai Road, Economic and Technological Development Zone, Qinhuangdao, Hebei Province, 066011, China

[2]sunCAE Consulting, Ginsterweg 3, 79194 Gundelfingen, Germany

[a]langyuling@dicastal.com, [b]suncae@unity-mail.de, [c]zhuzhihua@dicastal.com, [d]cixiang@dicastal.com, [e]kongdecai@dicastal.com, [f]qiaohaibo@dicastal.com, [g]wangwenbo1994@dicastal.com

Keywords: Casting aluminum alloy, Characterization, Damage model, Fatigue, Inhomogeneity, Simulation, Wheel, Knuckle.

Abstract. The purpose of the work is to quantify and predict the influence of inhomogeneity of local properties on the overall behavior of the selected casting aluminum wheel and knuckle in different loading cases. The investigated material is A356-T6. Smooth and notched tensile specimens and torsion specimens are extracted from different positions in the wheel and knuckle and tested. The dependences of the flow stress, the fracture strain, and the S-N curve on position for specimen extraction are evaluated. Metallographic investigations are performed to reveal the relations between microstructure/microdefects and the mentioned properties. A damage model based on a triaxiality-dependent fracture strain is calibrated and used to simulate the specimens and component tests. The simulations of static wheel tests and knuckle fatigue tests are performed with position-dependent material parameters. The prediction of the component tests is compared with the experimental results.

Introduction

The inhomogeneity of local mechanical properties across a casting aluminum component can significantly affect its mechanical behavior in real loading situations. A promising approach for a reliable prediction of the deformation and fracture behavior of cast components is a coupling between process simulations and structural simulations [1, 2] based on a quantitative description of the relations between microstructure and local properties. A relatively practicable approach is based on a direct characterization of mechanical properties for different positions and a subsequent component simulation with the data from the specimen tests [3, 4]. Since the damage behavior strongly depends on stress state, it is complicated to quantify both effects of stress state and inhomogeneity on component fracture behavior. Until now there are only a few published results about a systematic characterization of the effects [1]. An observable inhomogeneity of fatigue properties in casting aluminum components is depicted in [5, 6]. However, it is still a great challenge to find a reliable method to predict the fatigue behavior of the corresponding components taking the inhomogeneity into account.

In this work, a systematic characterization, component tests and numerical simulations on a casting aluminum alloy are performed to develop and to verify an evaluation method concerning component safety under different loadings. The specimens extracted from different positions of the wheel and the knuckle are tested to quantify the inhomogeneity of local properties of the wheel and knuckle. The mechanical properties of A356-T6 alloy are characterized using smooth tensile, notched tensile, and torsion tests. The fatigue tests are conducted under cyclic loading. Metallographic investigation of different parts is conducted to verify and to analyze the inhomogeneity of microstructure across the wheel and the knuckle. The position-dependent damage model and S-N curves used for components simulations are evaluated based on the specimen tests. The results of component simulations (wheel crack test, knuckle fatigue test) with position-dependent material parameters are verified by the comparison with the experimental results.

This article is an open access article under the terms and conditions of the Creative Commons Attribution (CC BY) license (https://creativecommons.org/licenses/by/4.0)

Characterization of Mechanical Properties of A356-T6 Alloy

Static tests on smooth tensile, notched tensile and torsion specimens. The samples were taken from wheels (18 inches, 16.8kg) with low-pressure die-casting A356 alloy subjected to T6 heat treatment. The main chemical composition of this alloy is shown in Table 1. Due to the complex geometry and inhomogeneous solidification rate in the wheel, seven positions were chosen for sampling different type specimens, as shown in Fig. 1. Smooth tensile specimens were tested according to DIN EN ISO 6892-1 on an Instron-8861 test machine at a strain rate of 10^{-3}/s and room temperature. The engineering stress-strain curves of smooth tensile specimens sampling from all seven positions are displayed in Fig. 1. It is visible that the fracture strain considerably scatters even within a series for the same specimen position. A trend for a position-dependence of the flow stress and fracture strain can be recognized despite the scatters. Through analyzing the uniaxial tensile mechanical properties of all seven positions, the notched tensile specimens and torsion specimens were finally sampled in only three positions (positions 1: spoke, 3: rim, and 5: hub). The average mechanical properties at three positions of the wheel are displayed in Table 2, including the average yield stress ($R_{p0.2}$), the average ultimate tensile strength (Rm), and the average elongation (Et). The experimental results of notched tensile tests are shown in Fig. 6 together with numerical results. The results of torsion tests are given in [1].

Table 1. Chemical compositions of A356-T6 alloy used in this work.

Elements	Si	Mg	Ti	Fe	Cu	Mn	Zn	Al
wt.%	6.8	0.25~0.45	0.13	0.10	<0.03	<0.03	<0.03	Bal.

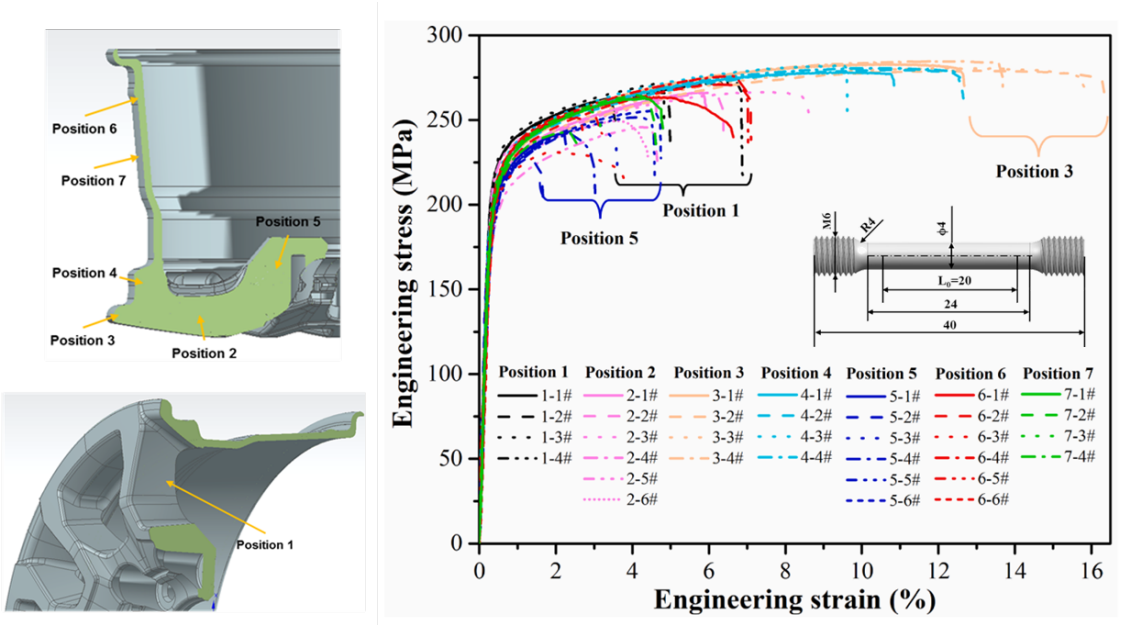

Fig. 1. Sampling positions in the wheel and the engineering stress-strain curves of smooth tensile specimens from 7 positions.

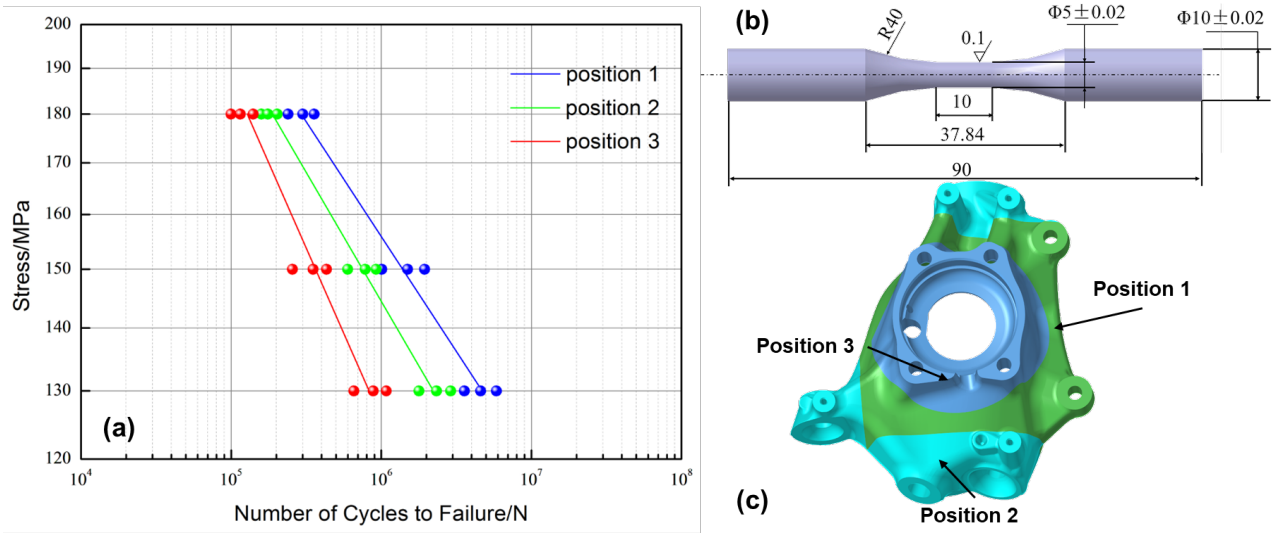

Fig. 2. (a) S-N curves at three different positions of one knuckle; (b) specimen geometry; (c) schematic diagram of sampling location.

Table 2. The average mechanical properties at different positions of the wheel and the knuckle.

Component	Position	$R_{p0.2}$ [MPa]	R_m [MPa]	Et [%]
Wheel	1	215.8 ± 4.8	268.2 ± 3.8	5.13 ± 1.72
	3	208.7 ± 5.5	281.9 ± 2.9	13.47 ± 1.16
	5	201.8 ± 3.8	244.3 ± 16.8	3.12 ± 1.52
Knuckle	1	267.5 ± 6.6	332.8 ± 5.6	8.26 ± 1.33
	2	268.7 ± 7.2	339.6 ± 6.8	9.97 ± 1.41
	3	271.3 ± 7.7	343.4 ± 9.3	11.69 ± 1.45

Fatigue tests on smooth specimens. The samples for the fatigue tests were taken from A356 knuckles (3.5kg) with counter-pressure die-casting and T6 heat treatment. The main chemical composition of this alloy is shown in Table 1. The sampling locations and fatigue specimen geometry (according to ASTM-E466 standard) are shown in Fig. 2(b, c). The average mechanical properties at three different positions of the knuckle are displayed in Table 2. The positions were selected based on the distance to the riser. It can be observed that the mechanical properties of the knuckle are better than the wheel. High-cycle fatigue tests were conducted on an electro-hydraulic servo fatigue testing machine (INSTRON8801). All specimens were tested at room temperature at the load ratio R=-1, and the frequency was 40Hz. Fig. 2(a) shows the S-N curves at three different positions of one steering knuckle. Obviously, the highest S-N curve is given by position 1 and the lowest S-N curve is from position 3. The k slope of position 1, 2, 3 is 8.5, 7.6, 5.7, respectively.

Metallographic investigation. The microstructure of the wheel in the three positions is shown in Fig. 3. It is observed that a typical hypoeutectic Al-Si alloy is formed by primary α-Al dendrites and eutectic Si particles. In addition, the cast pores (mostly shrinkage pores) could be obviously observed in position 1 and 5. This indicates that the high porosities in position 1 and 5 are the main reason for the lower strength and elongation of both positions in comparison with the values of position 3 where no big pores are visible. Fig. 4 shows the microstructure of different positions in one knuckle with different SDAS, where the measured SDAS of position 1 is 19.20 μm and position 3 is 40.07 μm. Obviously, a smaller SDAS in the casting alloy results in a higher S-N curve.

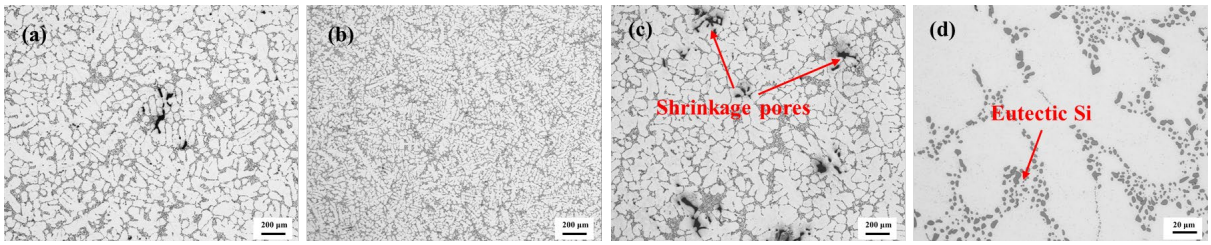

Fig. 3. The microstructure of (a) position 1 (spoke), (b) position 3 (rim), (c) position 5 (hub), (d) eutectic Si.

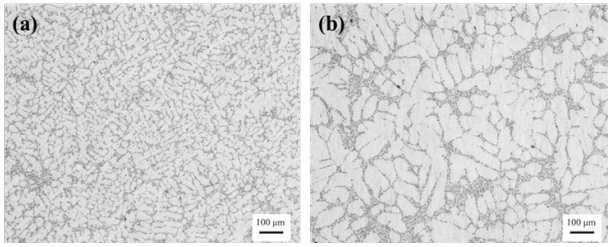

Fig. 4. Metallographic structure of different positions in one steering knuckle with different secondary dendrite arm spacings: (a) position 1, (b) position 3.

Modelling of Damage Behavior of Different Specimens

Damage model and its parameter determination. A damage model based on a triaxiality-dependent fracture strain [7] is applied to simulate the static tests. The fracture strain ε_f is defined as a function of the stress triaxiality σ_m/σ_e, which is the ratio of the mean stress σ_m to the von Mises effective stress σ_e. The values of triaxiality for torsion, uniaxial tension, and biaxial tension are zero, one-third, and two-thirds, respectively. The fracture occurs when the cumulative damage parameter D defined by Eq. 1 reaches the critical value of 1. Equation 1 shows the formula for the damage evolution, which can be used for a general non-linear damage accumulation:

$$\dot{D} = \frac{n}{\varepsilon_f^n}\ \varepsilon_p^{n-1}\ \dot{\varepsilon}_p \tag{1}$$

ε_p denotes the equivalent plastic strain, and the exponent n is a parameter controlling the damage evolution. For proportional loading, the integration of Eq. 1 leads to

$$D=(\varepsilon_p/\varepsilon_f)^n \tag{2}$$

The dependence of fracture stain ε_f on triaxiality σ_m/σ_e is determined by simulating the selected smooth and notched tensile tests and torsion tests and fitting the measured displacements at rupture. The fracture strain ε_f for each specimen type was taken from the equivalent plastic strain in the critical finite element showing the maximal damage variable D at the measured displacement at fracture. Since the fracture displacements of different specimens in a test series for the same specimen geometry usually lie in a scatter band, the averaged displacement at fracture was used for the fitting process. The corresponding triaxiality σ_m/σ_e for the determined fracture ε_f was also taken from the critical finite element.

Fig. 5 shows the determined fracture strains as a function of the corresponding triaxiality for the three different sampling positions. The developments of the local equivalent plastic strain in the critical elements in selected specimens are also given in Fig. 5 with solid lines for the whole loading period. The symbols represent the fracture strains determined from the individual tests. It is obvious that the fracture strain was not only influenced by triaxiality but also by sampling position. The study in [1] indicates that the microstructure and microdefect depend strongly on the position in the wheel. Position 1 (spoke) and position 5 (hub) show a much larger porosity than positions 3 (rim). The

fracture strain under both loading cases of tension and torsion decreases with increasing porosity [1]. The subsequent simulations of specimen and component tests are performed with the fracture strain vs. triaxiality curves in form of tables.

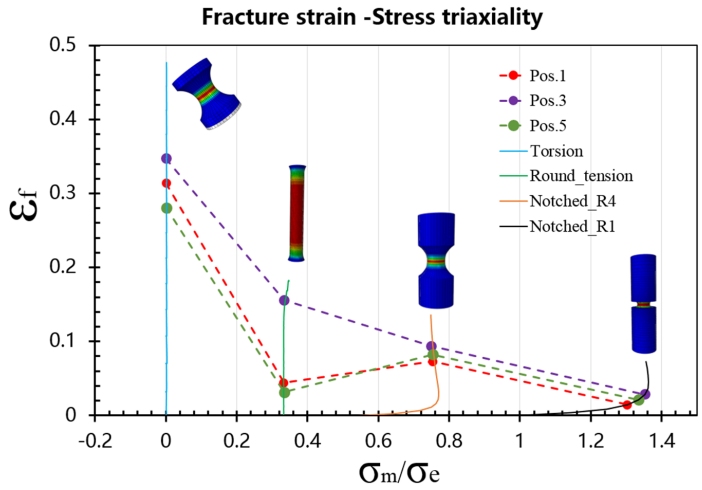

Fig. 5. Fracture strains as function of triaxiality for three positions in a wheel of A356-T6.

Simulation of specimen tests. The quasi-static tests on the smooth tensile specimens, the notched tensile specimens with a notch radius of 1 mm and 4 mm and the torsion specimens were simulated with Abaqus/Explicit, the specimens of which were extracted from three different positions (1, 3, 5). The hexahedral elements were used in the four FE models and the element edge length was about 0.2 mm. The specimen tests for each position were simulated with the true stress vs. true strain curve and the damage curve determined for the position.

The measured and calculated engineering stress vs. strain curves for smooth tensile and notched tensile (R1, R4) tests for three positions are shown in Fig. 6. The solid line represents the experimental curve, and the dashed line represents the simulation results. It can be observed that the wheel rim (position 3) shows the best material properties, with the highest strength and largest elongation. The worst part is the hub (position 5). The calculated stress vs. strain curves at different positions are consistent with the experimental results. The simulated engineering fracture strain in the torsion test shows high consistency with the experimental results as well [1].

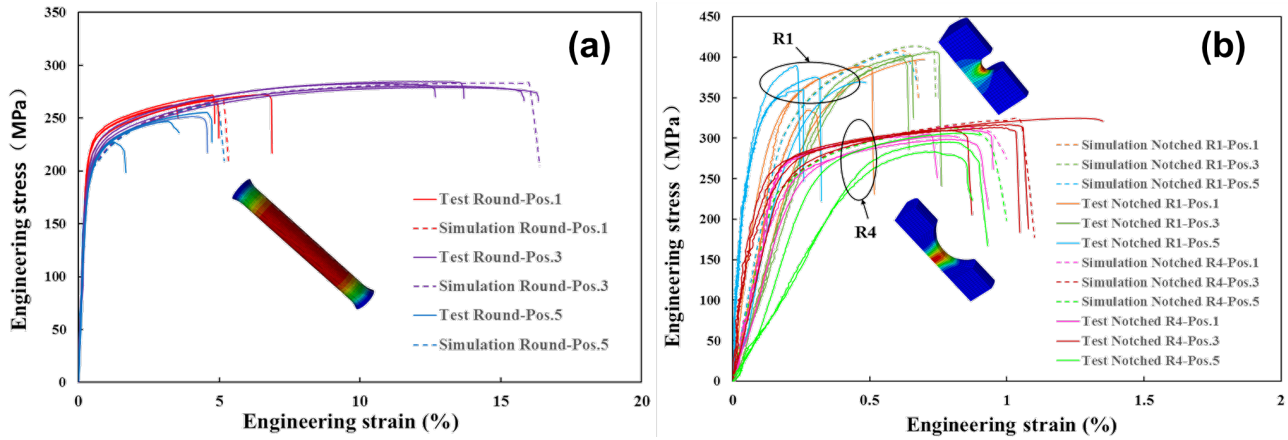

Fig. 6. Test and simulation results of (a) smooth tensile and (b) notched tensile specimens (R1, R4) for positions 1, 3, and 5 in the wheel.

Prediction of Damage Behavior of a Casting Aluminum Wheel and a Knuckle

The damage behavior of a wheel under static loading and the fatigue behavior of a knuckle under cyclic loading are simulated based on the material parameters discussed above. The effects of the inhomogeneity of local properties are taken into account.

Modeling of the damage behavior of a wheel under static loading. The wheel compression tests were performed at the Fraunhofer Institute for Mechanics of Materials IWM. As displayed in Fig. 7(a), one side of the wheel is in contact with a rigid wall. The other side is loaded slowly with a rigid device until the fracture of wheel. During the wheel test, the force vs. displacement curve was recorded and the deformation pattern was documented by a video film.

The simulation model for the wheel compression test was established to check the influence of position-dependent properties on the fracture behavior of the wheel. The software used for simulation is Abaqus/Explicit. As shown in the schematic figure (Fig. 7), one rigid body is fixed at one side. Another rigid body, set on the other side, moves towards the right at a speed of 0.5mm/s until the entire wheel is completely crushed.

The settings of the FE model are as follows. The material of the rigid body is steel. The wheel material is aluminum alloy A356 T6, with a mesh size of 5mm and the element type of C3D10M. The wheel is divided into three parts, named Pos.1 (orange area, spoke), Pos.3 (blue area, rim), and Pos.5 (green area, hub), as shown in Fig. 7(b). The damage parameters are given in Fig. 5.

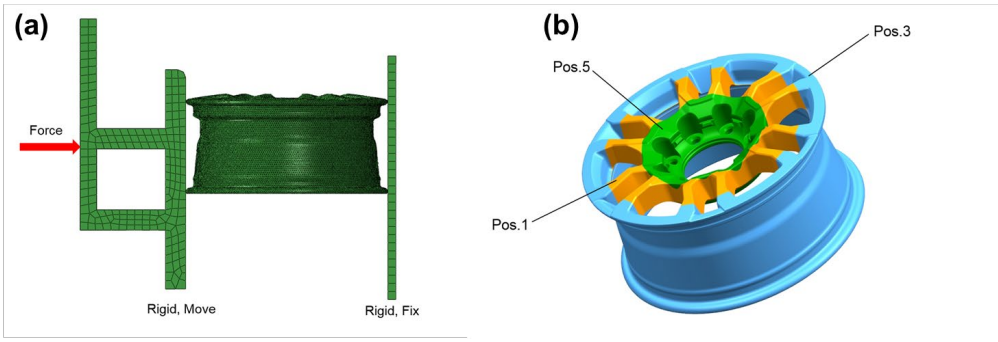

Fig. 7. (a) FE model of wheel compression test; (b) position-dependent material setting.

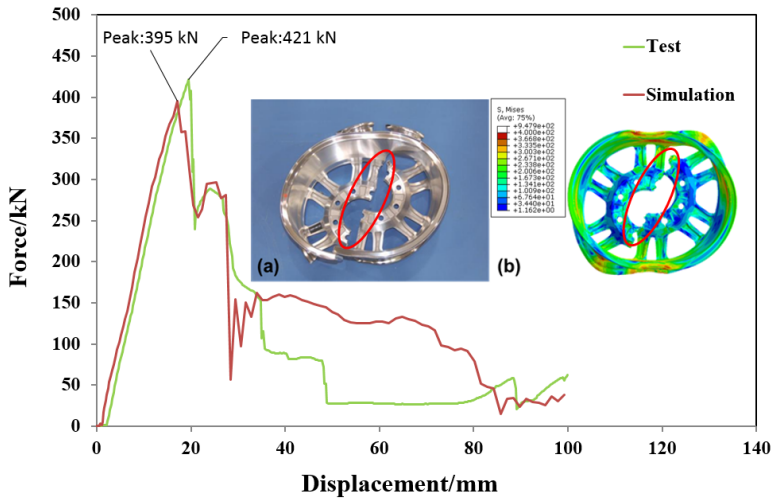

Fig. 8. Load vs. displacement curves and damage initiation (a) test (b) simulation.

The fracture behavior of the wheel in the compression test is compared between simulation and test in Fig. 8. The damage patterns from experiment and simulation are displayed in Fig. 8(a) and (b), respectively. It can be observed that the simulated and the experimental results of the wheel compression test are highly consistent, considering the crack location.

The force vs. displacement curves derived from the simulation and the test are also displayed in Fig. 8. The green line represents the curve recorded during the test, while the red line stands for the simulation result. The peak value represents the fracture force of the wheel, which characterizes the initiation of the fracture. The fracture force of the simulation and the test is 395kN and 421kN, respectively. Both the fracture force and the course of the curve from the simulation are in good agreement with the experimental results.

Modeling of the fatigue tests on a knuckle. The setup of the knuckle fatigue test is shown in Fig. 9. The knuckle is fixed at the wheel center. The cyclic load, which is 15kN, is applied to the steering arm at X-Y plane with the direction of 90° to the clamping surface. The load frequency is 10Hz. The crack location and fatigue cycles are recorded during the experiment. Totally three repeated tests were conducted.

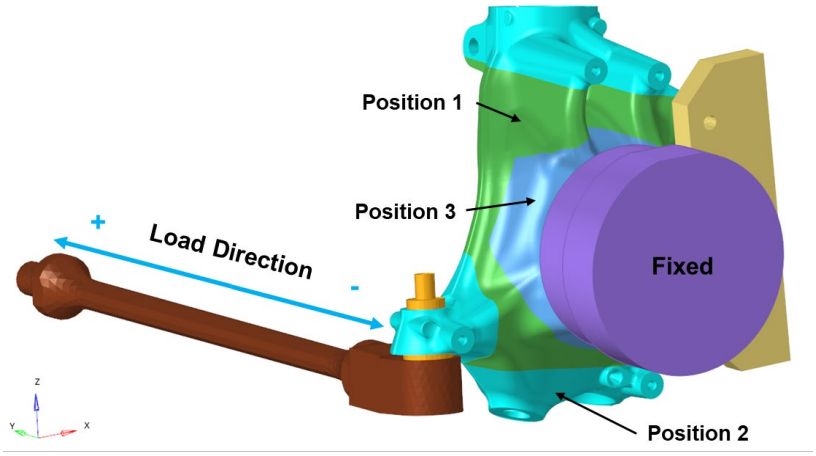

Fig. 9. FE-Model of knuckle fatigue test.

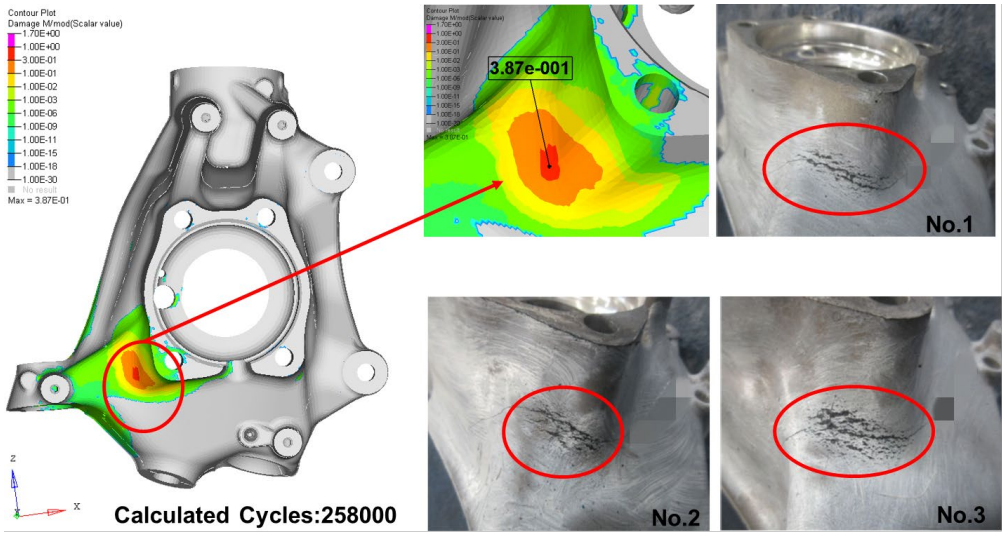

Fig. 10. Calculated and experimental results of knuckle fatigue tests.

To verify the applicability of the position-dependent S-N curves, the FE model was set up in accordance with the test. The damage was calculated with Abaqus/Standard and FEMFAT. The inhomogeneity of local mechanical properties was considered by dividing the knuckle into three parts, as shown in Fig. 9. The position-dependent material card is based on the results given in Fig. 2. The tetrahedral elements were used in the FE-model with the element size of 2mm. The load cycles defined in the FEMFAT are 100000.

The simulated and experimental results are displayed in Fig. 10, including the position with the maximum damage from simulation and the crack locations from 3 different knuckle tests. It can be observed that the simulation results are highly consistent with the experimental results in predicting the crack location.

The simulation result is further validated based on the comparision of fatigue life. The calculated maximum damage is 0.382. Life is the reciprocal of damage, which is 2.58. According to the input cycles in FEMFAT, the fatigue cycles are calculated to be 258000. The experimental cycles at crack initiation and the logarithmic error are displayed in Table 3. The logarithmic error of the fatigue test is -2.16%, 1.40%, and 2.05%, respectively, indicating a good agreement between the simulation and the test.

Table 3. Fatigue test cycles.

No.	Test cycles	Calculated cycles	Log error [%]
1	197106	258000	-2.16
2	307290		1.40
3	333263		2.05

Conclusions

The characterization of different positions in the investigated casting aluminum components shows a strong inhomogeneity of mechanical properties. The ultimate tensile strength averaged from three positions in the casting wheel of A356 T6 changes from 244.2 MPa to 281.9 MPa. The average elongation changes from 3.12% to 13.47%. The metallographic investigation delivers the indication that the microstructure (e.g., SDAS) and microdefects (e.g., porosity) considerably affect the strength, fracture strain and fatigue life.

A damage model based on a triaxiality-dependent fracture strain was calibrated by simulating different tests on smooth and notched tensile specimens and torsion specimens extracted from three positions (spoke, rim, hub) in a casting wheel. The FE model for the wheel consisted of three material zones with the corresponding stress vs. strain curves and damage parameters. Both the measured force vs. displacement curves of the static wheel tests and the damage positions in the tested wheel were well predicted by the simulation with the applied position-dependent material parameters.

Fatigue tests on a casting aluminum knuckle were simulated and the damage was calculated with Abaqus/Standard and FEMFAT. The inhomogeneity of local mechanical properties was considered by dividing the FE model for the knuckle into three material parts. The corresponding S-N curve was used for each part. The calculated fatigue cycles and damage positions agree with the experimental results of the knuckle tests very well.

Acknowledgment

We are very grateful to the experts of the Institute of Metal Research, Chinese Academy of Sciences, Shenyang, and the Fraunhofer Institute for Mechanics of Materials IWM, Freiburg, Germany who supported this work.

References

[1] D. Kong, D.-Z. Sun, B. Yang, H. Qiao, C. Wei, Y. Lang, H. Song, J. Gao, Engineering Failure Analysis 145 (2023) 107018.

[2] F. Andrieux, D.-Z. Sun, A. Burblies, ALUMINIUM TWO THOUSAND, 10th International Congress & ICEB, 6th International Conference on Extrusion and Benchmark, Verona – Italy, 20 – 24 June 2017.

[3] Y. Leost, A. Sonntag, T. Haase, Modeling of a cast aluminum wheel for crash application, 11th European LS-DYNA Conference 2017, Salzburg Austria.

[4] G. Previati, F. Ballo, M. Gobbi, G. Mastinu, Radial impact test of aluminium wheels numerical simulation and experimental validation, Int. J. of Impact Engineering, 126, 117-134, 2019.

[5] B. Yang, S. Chen, H. Song, S. Zhang, H. Chang, S. Xu, Z. Zhu, C. Li, Mater. Sci. Eng., A 857 (2022) 144106.

[6] R. Hidalgo, J.A. Esnaola, I. Llavori, M. Larrañaga, I. Hurtado, N. Herrero-Dorca, Int. J. of Fatigue 125 (2019) 468–478.

[7] D.-Z. Sun, A. Ockewitz, F. Andrieux, H. Klamser, Proc. of the 12th Int. Conference on Aluminium Alloys, September 5-9, 2010, Yokohama, Japan, ©2010 The Japan Institute of Light Metals.